

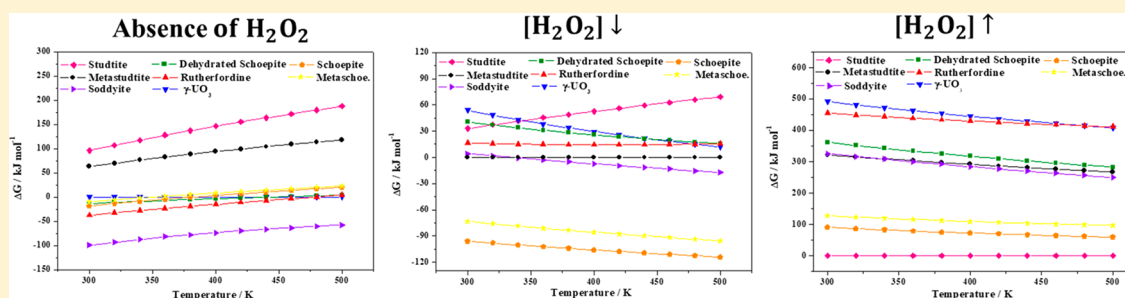
Periodic DFT Study of the Thermodynamic Properties and Stability of Schoepite and Metaschoepite Mineral Phases

Francisco Colmenero,^{*,†} Ana María Fernández,[‡] Joaquín Cobos,[‡] and Vicente Timón[†]

[†]Instituto de Estructura de la Materia (IEM-CSIC), C/Serrano, 113, 28006 Madrid, Spain

[‡]Centro de Investigaciones Energéticas, Medioambientales y Tecnológicas (CIEMAT), Avda/Complutense, 40, 28040 Madrid, Spain

S Supporting Information



ABSTRACT: The thermodynamic properties of schoepite and metaschoepite were obtained by means of theoretical solid-state methods as a function of temperature. Since the values of these properties for schoepite have not been measured experimentally, they were predicted. The computed thermodynamic functions of metaschoepite were in excellent agreement with the experimental information. These functions were used to obtain the thermodynamic properties of formation of these materials from the corresponding elements. The calculated Gibbs free energy of formation of metaschoepite was shown to be very reliable and differ from the experimental value at 800 K by only 2.0%. Besides, it extends the range of temperature in which this property is known to 0–1000 K. Then, these properties were combined with those of other important uranyl-containing materials to study the reactions of formation of schoepite and metaschoepite from uranium trioxide and the reactions of transformation of these materials into dehydrated schoepite, rutherfordine, and soddyite. Schoepite becomes unstable with respect to uranium trioxide for temperatures higher than 110 °C (383 ± 27 K) and its dehydration occurs at 64 °C (337 ± 44 K). The corresponding values of these temperatures for metaschoepite are 82 °C (355 ± 6 K) and 5 °C (278 ± 9 K), respectively. Under hydrogen peroxide free conditions, schoepite and metaschoepite were found to be less stable than rutherfordine and soddyite. The thermodynamic stability of schoepite with respect to metastudtite and studtite was then studied under different conditions of temperature and concentrations of hydrogen peroxide. Schoepite and metaschoepite have very similar thermodynamic stabilities, the first being slightly more stable than the second one. The availability of the thermodynamic properties of these minerals allowed to determine their relative thermodynamic stability with respect to a rich subset of the most relevant secondary phases resulting from corrosion of spent nuclear fuel. Schoepite and metaschoepite were found to be the first and second most stable phases under intermediate hydrogen peroxide concentrations and the second and third most stable phases under high concentrations of hydrogen peroxide, respectively.

KEYWORDS: spent nuclear fuel, schoepite, DFT, thermodynamic properties, Gibbs free energies of reaction, thermodynamic stability

I. INTRODUCTION

Schoepite, $[(\text{UO}_2)_8\text{O}_2(\text{OH})_{12}] \cdot 12 \text{H}_2\text{O}$, and metaschoepite, $[(\text{UO}_2)_8\text{O}_2(\text{OH})_{12}] \cdot 10 \text{H}_2\text{O}$ ^{1–9} (also referred to as $\text{UO}_3 \cdot 2.25 \text{H}_2\text{O}$ and $\text{UO}_3 \cdot 2 \text{H}_2\text{O}$, respectively), have been identified as basic components of the paragenetic sequence of secondary phases arising from the alteration of natural uraninites and corrosion of spent nuclear fuel (SNF) under final geological disposal (FGD) conditions.^{10–17} Although the formation of these mineral phases should occur in a radioactive nuclear waste repository (RNWR) placed in an oxidizing environment,^{15–17} these phases are also relevant even in the case of RNWRs placed in reducing environments. While the ground-

water conditions in a nuclear radioactive waste disposal will be generally reducing, an oxidative environment has been hypothesized in a 50 μm -layer near the fuel surface.¹⁸ These oxidant conditions are a consequence of the radiolysis of water due to the action of intense ionizing radiation linked to the spent fuel^{19,20} leading to the generation of oxidants as hydrogen peroxide, H_2O_2 .²¹ The formation of uranyl peroxide

Received: August 10, 2018

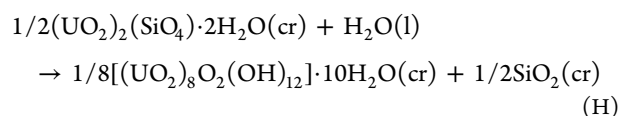
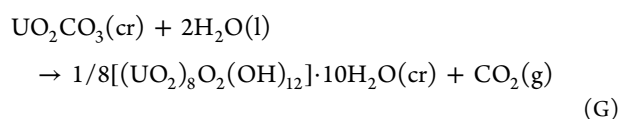
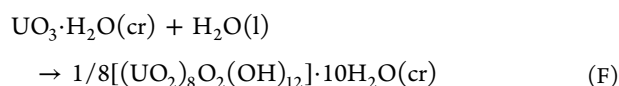
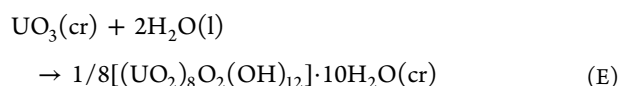
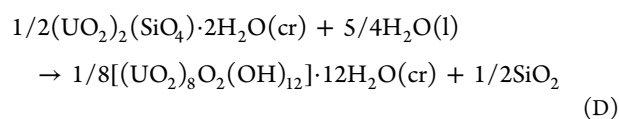
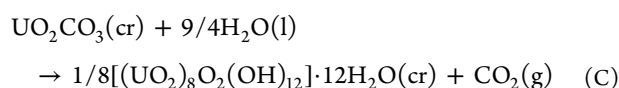
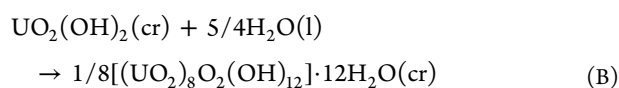
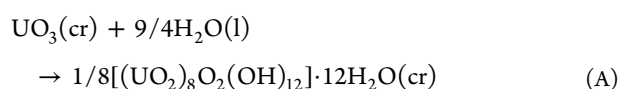
Revised: December 1, 2018

Accepted: December 5, 2018

Published: December 5, 2018

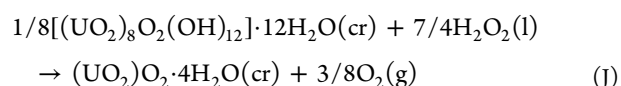
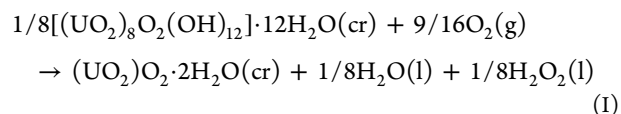
and oxyhydroxide phases will follow from the contact of these oxidants with uranium dioxide.^{22,23} Schoepite and metaschoepite phases have been identified on the “lava” formed after the Chernobyl nuclear accident²⁴ and as corrosion products of SNF in the cooling basins at the Hanford nuclear facility.^{25–27}

In this Article, the fundamental thermodynamic properties (TP) of schoepite and metaschoepite minerals, including their temperature dependence, have been obtained by using theoretical solid-state methods based on density functional theory using plane waves and pseudopotentials.²⁸ Once the TPs of these materials were known, they were employed in order to derive the thermodynamic properties of formation (TPF) of these uranyl-containing materials (UCM) in terms of the elements using the methods developed in recent works.^{29,30} These TPFs were then combined with those of dehydrated schoepite ($\text{UO}_2(\text{OH})_2$), soddyite ($(\text{UO}_2)_2(\text{SiO}_4) \cdot 2\text{H}_2\text{O}$), rutherfordine (UO_2CO_3), and gamma uranium trioxide ($\gamma\text{-UO}_3$), reported in a previous paper²⁹ to study eight reactions involving schoepite and metaschoepite and these materials:

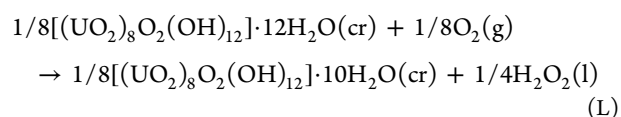
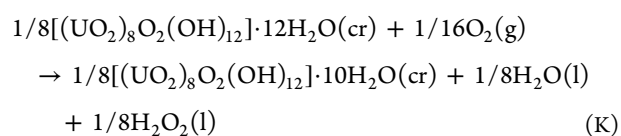


The reactions (A) to (D) describe the formation of schoepite in terms of the uranium trioxide and the transformations of dehydrated schoepite, rutherfordine, and soddyite minerals into schoepite, respectively. Reactions (E) to (H) are analogous to the previous reactions but for metaschoepite. Because, with the exception of reaction (E), the experimental values of the TPs of these important reactions are not known, our theoretical calculations have allowed to predict the corresponding enthalpies and Gibbs free energies of reaction (EOR and GFEOR) and associated reaction constants (RC) for an extended range of temperature. The relative thermodynamic stability (TS) of schoepite with respect to the

uranyl peroxide hydrates, metastudtite ($(\text{UO}_2)_2\text{O}_2 \cdot 2\text{H}_2\text{O}$) and studtite ($(\text{UO}_2)_2\text{O}_2 \cdot 4\text{H}_2\text{O}$), in the presence of H_2O_2 and water and under high H_2O_2 concentrations, respectively, were then analyzed by studying the following reactions:



Similarly, the relative TSs of metaschoepite with respect to schoepite in the presence of H_2O_2 and water and under high H_2O_2 concentrations, respectively, were determined by studying the following transformation reactions:



These results extend a previous work³⁰ in which the TPs of a large set of reactions including other UCMs were obtained. These TP functions are important inputs for the performance assessment (PA) calculations of RNWRs because the relative TS of the secondary phases of SNF under FGD conditions is highly temperature dependent.³⁰ Furthermore, combining the thermodynamic data obtained with those achieved in the previous paper,³⁰ the relative stability of schoepite and metaschoepite with respect to a subset of the most important secondary phases appearing in the surface of SNF under FGD conditions has been investigated.

This Article is organized in the following manner. The theoretical methodology employed is described in Section II. The main results of this Article are given and discussed in Section III. Subsection III.1 provides the TPs of schoepite and metaschoepite mineral phases obtained by means of periodic density functional theory employing plane waves and pseudopotentials.²⁸ The calculated TPFs of schoepite and metaschoepite are reported in Subsection III.2. Subsections III.3.a and III.3.b contain the results for the EOR and GFEOR of reactions (A) to (D) and (E) to (H), respectively. The thermodynamic properties of the reaction (TPRs) of dehydration of schoepite into metaschoepite are reported in Subsection III.3.c, and those of reactions (I) to (L) are given in Subsection III.3.d. The results allowed to determine the relative TS of schoepite and metaschoepite with respect to a series of the most important secondary phases of the SNF under different conditions.³⁰ Hence, the TS of schoepite and metaschoepite phases is discussed in Subsection III.4. The solubility products of schoepite and metaschoepite are studied in Subsection III.5. Finally, the main conclusions of this Article are presented in the Section IV.

II. METHODS

II.1. Thermodynamic Properties. The crystal structures of schoepite and metaschoepite mineral phases were modeled

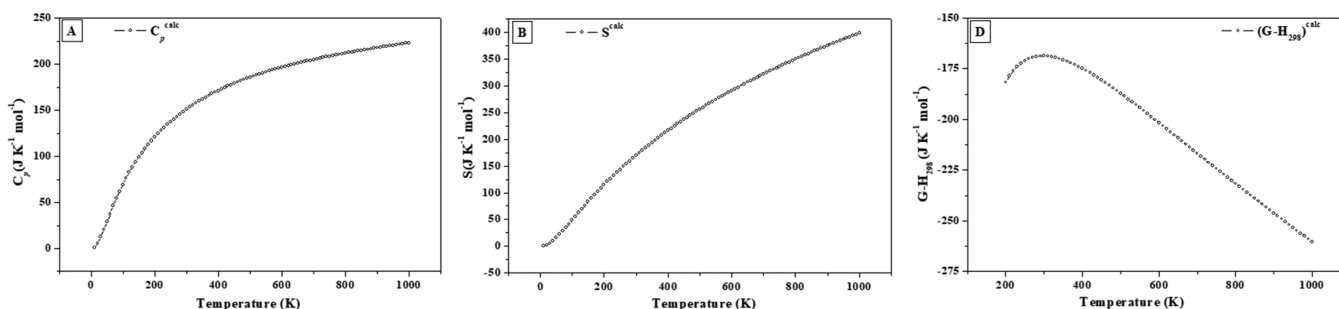


Figure 1. Computed heat capacity (A), entropy (B), and Gibbs free energy (C) functions of schoepite.

using the CASTEP code,³¹ included in the Materials Studio package of programs.³² The DFT-D2 approach,³³ that is, the PBE density functional³⁴ supplemented with the Grimme empirical dispersion correction, was employed. The inclusion of dispersion corrections improved significantly the description of the dense hydrogen bond network present in the unit cell structures of these materials. The pseudopotentials employed for O and H atoms were standard norm-conserving pseudopotentials³⁵ included in CASTEP program. For uranium atom a new norm-conserving relativistic pseudopotential,^{36,37} used extensively in the research of UCMs,^{36–43,29,30} was employed in the calculations. The thermodynamic properties of some uranyl containing materials such as dehydrated schoepite, studtite, and metastudtite have also been determined using theoretical solid-state methods by Weck and Kim^{44,45} and Sassani et al.⁴⁶ The reaction enthalpies of some reactions involving some uranium fluorides and oxides were determined theoretically by Beridze and Kowalski.⁴⁷

The details of the computational treatment of schoepite were described in a previous article,⁴³ and those corresponding to metaschoepite are given in an Appendix of the [Supporting Information](#). The calculations were carried out with two different values of the kinetic cutoff, 750 and 950 eV, to study the variation of the computed properties with respect to the increase of this calculation parameter. Since the variation was small, the calculations performed with the cutoff value of 950 eV were considered to be well converged, and the corresponding results were reported here. The structural results and the X-ray diffraction pattern obtained for schoepite in the previous work⁴³ and provided in the Appendix of the [Supporting Information](#) for metaschoepite are in very good agreement with their experimental counterparts. The linear response density functional perturbation theory (DFPT)^{48–52} implemented in the CASTEP code was also used in order to determine the Raman spectra of schoepite. The computed Raman spectrum of schoepite was in very good agreement with the one recorded experimentally.⁴³

In order to determine the TPs of these materials, phonon calculations were carried out at the optimized structures of schoepite and metaschoepite. The phonon spectrum at the different points of Brillouin zone were obtained employing the density functional perturbation theory (DFPT) technique as second order derivatives of the total energy.⁴⁸ The phonon dispersion curves and density of states were computed from the phonon spectra, and from them, several important TPs in the quasi-harmonic approximation, such as Gibbs free energies, enthalpies, entropies, specific heats and Debye temperatures were evaluated.^{53,48}

II.2. Thermodynamic Properties of Formation. The enthalpies and Gibbs free-energies of formation (EOF and

GFEF) of schoepite and metaschoepite were determined, from the computed enthalpy and entropy functions, $(H_T - H_{298})^{\text{calc}}$ and S_T^{calc} , by means of the relationships:^{29,54}

$$\Delta_f H(T) = \Delta_f H^\circ + (H_T - H_{298})^{\text{calc}} - \sum_i^{\text{elements}} n_i (H_T - H_{298})_i^{\text{exp}} \quad (1)$$

$$\Delta_f G(T) = \Delta_f H(T) - T \left\{ S_T^{\text{calc}} - \sum_i^{\text{elements}} n_i (S_T)_i^{\text{exp}} \right\} \quad (2)$$

In these equations, $\Delta_f H^\circ$ is the EOF at the standard state (at the temperature of 298.15 K and a pressure of 1 bar) of the material being considered, and $(H_T - H_{298})_i^{\text{exp}}$ and $(S_T)_i^{\text{exp}}$ are the enthalpy and entropy functions of the elements forming part of this material with stoichiometric coefficients n_i , respectively. The precise values used for $\Delta_f H^\circ$ will be given below. The thermodynamic functions for hydrogen and oxygen were obtained from JANAF (Joint Army-Navy-Air Force) thermochemical tables,⁵⁴ and those for uranium were obtained from Barin.⁵⁵ The RCs of the formation reactions were calculated from the corresponding Gibbs free energies of formation employing the relationship:⁵⁴

$$\Delta G(T) = -RT \ln K \quad (3)$$

II.3. Thermodynamic Properties of Reaction. The EORs and GFEORs at different temperatures were obtained using our computed EOF and GFEF functions,³⁰ $\Delta_f G(T)^{\text{calc}}$ and $\Delta_f S(T)^{\text{calc}}$, by means of the expressions:⁵⁴

$$\Delta_r G(T) = \sum_i^{\text{products}} n_i \Delta_f G^i(T) - \sum_j^{\text{reactants}} n_j \Delta_f G^j(T) \quad (4)$$

$$\Delta_r H(T) = \Delta_r G(T) + T \cdot \Delta_r S(T) \quad (5)$$

where,

$$\Delta_r S(T) = \sum_i^{\text{products}} n_i \Delta_f S^i(T) - \sum_j^{\text{reactants}} n_j \Delta_f S^j(T) \quad (6)$$

In these relations, $\Delta_f G^i(T)$ and $\Delta_f S^i(T)$, are the GFEF and entropy of formation at temperature T of compound i participating in the reaction with stoichiometric coefficient n_i . The precise values used of the TP functions for dehydrated schoepite, metastudtite, studtite, soddyite, rutherfordine, and $\gamma\text{-UO}_3$ were obtained in a previous paper.²⁹ The TP functions for $\text{SiO}_2(\text{cr})$, $\text{H}_2\text{O}(\text{l})$, $\text{O}_2(\text{g})$, and $\text{CO}_2(\text{g})$ were obtained from JANAF thermochemical tables,⁵⁴ and those for $\text{H}_2\text{O}_2(\text{l})$ were obtained from Barin.⁵⁵ The RCs were obtained, as in

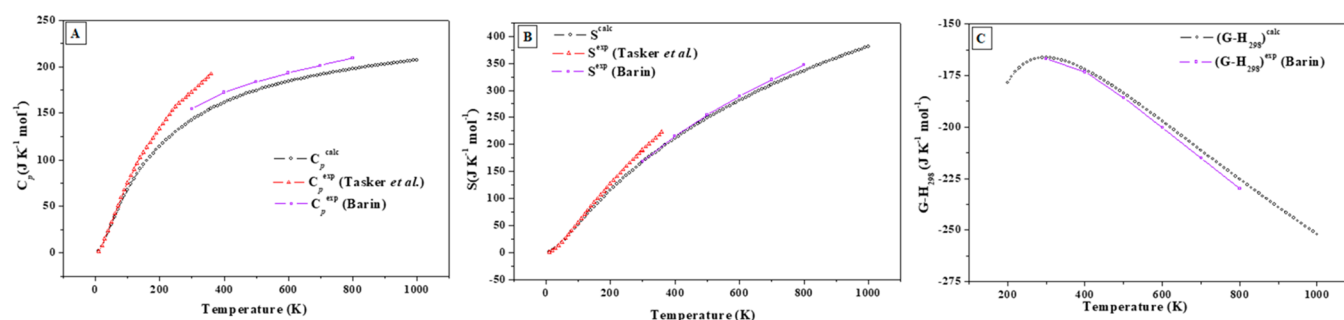


Figure 2. Computed heat capacity (A), entropy (B), and Gibbs free energy (C) functions of metaschoepite. The experimental values were reported by Tasker et al.⁵⁶ (in red) and Barin⁵⁵ (in violet).

Table 1. Comparison of the Calculated TPs of Schoepite and Metaschoepite at the Temperature of 298.15 K and the Corresponding Experimental Data for Metaschoepite^{55,56a}

	property	C_p	S	$H_T - H_{298}$	$G_T - H_{298}$
schoepite	calc.	150.62	168.75	0	-168.75
metaschoepite	calc.	142.01	166.24	0	-166.24
	exp. ⁵⁶	172.07 ± 0.34	188.54 ± 0.38	0	-188.54 ± 0.38
	exp. ⁵⁵	154.40	167.00	0	167.00

^aAll the values of the TPs are given in units of $\text{J}\cdot\text{K}^{-1}\cdot\text{mol}^{-1}$.

Subsection II.2, from the GFEORs by means of the well-known eq 3.

III. RESULTS AND DISCUSSION

III.1. Thermodynamic Properties of Schoepite and Metaschoepite. *III.1.a. Schoepite.* Phonon calculations were performed at the optimized structure of schoepite. The TPs were evaluated from the computed phonon spectra. Figure 1A–C display the computed isobaric heat capacity (C_p), entropy, enthalpy, and Gibbs free energy functions, respectively. The values of enthalpy and Gibbs free energy were divided by the temperature to express these properties using the same units as for C_p and S ($\text{J}\cdot\text{K}^{-1}\cdot\text{mol}^{-1}$). The values of the computed TPs over the temperature range 0–1000 K are given in Tables S.1 to S.4 of the Supporting Information.

Since the TPs of schoepite have not been measured experimentally, their values were predicted. The calculated values of the isobaric specific heat and entropy at 298.15 K are $C_p = 150.62 \text{ J}\cdot\text{K}^{-1}\cdot\text{mol}^{-1}$ and $S = 168.75 \text{ J}\cdot\text{K}^{-1}\cdot\text{mol}^{-1}$. The calculated values of the TPs of schoepite at selected temperatures are given in Tables S.9 and S.10 of the Supporting Information. The calculated isobaric specific heat at the last temperature considered in the present work (1000 K), $C_p = 223.2 \text{ J}\cdot\text{K}^{-1}\cdot\text{mol}^{-1}$, is 16.7% below the corresponding Dulong–Petit asymptotic limit ($C_p = 268.1 \text{ J}\cdot\text{K}^{-1}\cdot\text{mol}^{-1}$).

III.1.b. Metaschoepite. From the corresponding phonon calculations for metaschoepite, performed at its optimized equilibrium structure, the TPs were evaluated. Figures 2A–C display the computed isobaric heat capacities, entropies, and Gibbs free energies, respectively. The precise values of these TPs over the temperature range 0–1000 K are provided in Tables S.5 to S.8 of the Supporting Information.

Although the range of thermal stability of metaschoepite appears to be from 0 to 425 K,⁵⁶ it will be shown below that the thermal stability of metaschoepite in the presence of H_2O_2 is much larger. For this reason, the values of the TPs of this material are provided in Tables S.5 to S.8 of the Supporting Information and shown in Figure 2 for the extended range of temperatures from 0 to 1000 K. The calculated isobaric specific

heat at the last temperature considered in the present work (1000 K), $C_p = 207.1 \text{ J}\cdot\text{K}^{-1}\cdot\text{mol}^{-1}$ is 17.1% below the Dulong–Petit asymptotic value ($C_p = 249.9 \text{ J}\cdot\text{K}^{-1}\cdot\text{mol}^{-1}$).

The results for the TPs of metaschoepite at 298.15 K are compared with the corresponding experimental data reported by Tasker et al.⁵⁶ and Barin⁵⁵ in Table 1. While the agreement with the experimental data of Tasker⁵⁶ is only reasonable, the agreement with those of Barin⁵⁵ is very good. The calculated isobaric specific heat of metaschoepite is, as expected, lower than the corresponding calculated specific heat of schoepite by about 6.1%. The values measured by Tasker et al.⁵⁶ may be inaccurate probably due to impure starting materials with water content that is intermediate between that of schoepite and metaschoepite.

It must be emphasized that Tasker et al.⁵⁶ used, even in the title of their article, the name “schoepite” to refer to a material with formula, $\text{UO}_2(\text{OH})_2\cdot\text{H}_2\text{O} \equiv \text{UO}_3\cdot 2\text{H}_2\text{O}$ (metaschoepite). As may be seen in their article, the lattice parameters associated with their sample ($a = 13.977 \text{ \AA}$; $b = 16.696 \text{ \AA}$; $c = 14.672 \text{ \AA}$) agree with those of metaschoepite (after a change of the names of the axes). Besides, the authors state that the X-ray diffraction pattern of their sample was identical to that of Debets and Loopstra,⁵⁷ which corresponds again to metaschoepite, not schoepite.

A comparison of the calculated TPs of schoepite and metaschoepite with the corresponding experimental data for metaschoepite measured by Tasker et al.⁵⁶ in the range of temperatures from 0 to 360 K is provided in Tables S.9 and S.10 (see Supporting Information). Similarly, the experimental values of the heat capacity, entropy, enthalpy and Gibbs free energy for metaschoepite reported by Barin⁵⁵ in the range of temperatures from 298.15 to 800 K are compared with the calculated data in Tables S.11 and S.12 (see Supporting Information). The last experimental value of the isobaric specific heat reported by Tasker et al.⁵⁶ at $T = 360 \text{ K}$ ($C_p = 199.9 \text{ J}\cdot\text{K}^{-1}\cdot\text{mol}^{-1}$) is about 20.0% below the Dulong–Petit asymptotic value. Likewise, the experimental value of the isobaric specific heat reported by Barin⁵⁵ at $T = 800 \text{ K}$ ($C_p = 208.84 \text{ J}\cdot\text{K}^{-1}\cdot\text{mol}^{-1}$) is 16.4% below the asymptotic limit. As

Table 2. Experimental, Assessed, and Estimated Values of the GFEOf of Schoepite and Metaschoepite at the Standard State^a

material	ref	type of data	$\Delta_f G^0$
Metaschoepite	Langmuir ⁵⁸	assessed	-1633.4
	Hemingway ⁵⁹	experimental	-1632.0 ± 4.0
	Finch ⁶⁰	estimated	-1636.50 ± 5.0
	O'Hare et al. ⁶¹	assessed	-1637.0 ± 1.7
	Barin ⁵⁵	experimental	-1630.662
	Tasker et al. ⁵⁶	experimental	-1636.51 ± 1.7
	Grenthe et al. ⁶²	assessed	
	Guillaumont et al. ⁶³	assessed	
	Kubatko et al. ⁶⁴	derived ^b	-1601.4 ± 3.1
	Gorman-Lewis et al. ^{65,66}	experimental	-1632.2 ± 7.4
Schoepite	Finch ⁶⁰	estimated	-1697.15 ± 5.0

^aThe GFEOf values are given in units of $\text{kJ}\cdot\text{mol}^{-1}$. ^bObtained from the value of the EOF at the standard state measured by Kubatko et al.⁶⁴ and the experimental value of the metaschoepite entropy reported by Tasker et al.⁵⁶

can be seen, the difference between the experimental results of Tasker et al.⁵⁶ with respect to the experimental ones of Barin⁵⁵ and the calculated results increase as the temperature increases. The same is not true for the experimental TPs reported by Barin,⁵⁵ which agree well with the calculated properties even at temperatures of the order of 800 K. The percent differences of the calculated specific heat, entropy, and Gibbs free energy with the experimental results of Barin⁵⁵ are 8.0%, 4.6%, and 4.6% at 298.15 K and become 5.4%, 3.2%, and 2.0% at 800 K, respectively (see Tables S.11 and S.12 of the Supporting Information). Whereas the TPs reported by Barin⁵⁵ seems to be accurate, the TPs computed in this work are recommended because they expand the temperature range in which they are known from 298.15–800 K to 0–1000 K.

III.2. Thermodynamic Properties of Formation.

III.2.a. Standard State EOF and GFEOf of Schoepite and Metaschoepite. The experimental values of the standard state GFEOf and EOF of metaschoepite are summarized in Tables 2 and 3,^{55,56,58–67} respectively. There are not experimental values for the standard state EOF of schoepite, a quantity required to evaluate the temperature dependence of the GFEOfs and EOFs.^{29,30} Nevertheless, an estimate of $\Delta_f H^0$

Table 3. Experimental, Assessed, and Estimated Values of the EOF of Schoepite and Metaschoepite at the Standard State^a

material	ref	type of data	$\Delta_f H^0$
Metaschoepite	Cordfunke ⁶⁷	experimental	-1829.7
	Langmuir ⁵⁸	assessed	-1825.9
	Hemingway ⁵⁹	experimental	-1826.0 ± 4.0
	O'Hare et al. ⁶¹	assessed	-1826.4 ± 2.1
	Barin ⁵⁵	experimental	-1826.701
	Tasker et al. ⁵⁶	experimental	-1826.1 ± 1.7
	Grenthe et al. ⁶²	assessed	
	Guillaumont et al. ⁶³	assessed	
	Kubatko et al. ⁶⁴	experimental	-1791.0 ± 3.2
	Gorman-Lewis et al. ⁶⁵	derived ^b	-1825.8 ± 7.4
Schoepite	This work	estimated ^c	-1910.05 ± 5.0

^aThe EOF values are given in units of $\text{kJ}\cdot\text{mol}^{-1}$. ^bObtained from the value of the GFEOf at the standard state measured by Gorman-Lewis et al.⁶⁵ and the experimental value of the metaschoepite entropy reported by Tasker et al.⁵⁶ ^cObtained by using the GFEOf estimated by Finch⁶⁰ and our calculated value of the schoepite entropy at 298.15 K.

may be obtained from the value reported by Finch⁶⁰ for the standard state GFEOf of schoepite (see Table 2). From this value and our calculated value of the entropy of schoepite at 298.15 K (Table 1), we obtained the final value $\Delta_f H^0(\text{UO}_3 \cdot 2.25 \text{H}_2\text{O}(\text{cr})) = -1910.05 \pm 5 \text{kJ}\cdot\text{mol}^{-1}$, which is the value used in the present work. Since the method of estimation of Finch^{60,68,69} was also applied to the metaschoepite mineral, we could evaluate its accuracy by comparing the result for the $\Delta_f G^0$ of metaschoepite with the corresponding experimental values. As observed in Table 2, the value differs from the experimental metaschoepite standard state GFEOf values by at most $\pm 5 \text{kJ}\cdot\text{mol}^{-1}$. This error estimation seems to be too small if we consider the experimental standard state EOF of metaschoepite reported by Kubatko et al.⁶⁴ However, as discussed in the next paragraph, this value seems to be inconsistent with respect to the value of the standard state GFEOf measured by Gorman-Lewis et al.⁶⁵

The assessed value of $\Delta_f G^0$ for metaschoepite of Kubatko et al.⁶⁴ given in Table 2, corresponding to the value $\Delta_f H^0 = -1791.0 \pm 3.2 \text{kJ}\cdot\text{mol}^{-1}$ measured experimentally by these authors⁶⁴ (see Table 3), was calculated from this $\Delta_f H^0$ value and the standard state entropy reported by Tasker et al.⁵⁶ (Table 1). This yields a value $\Delta_f G^0 = -1601.4 \pm 3.1 \text{kJ}\cdot\text{mol}^{-1}$, which is very different from the rest of the values given in Table 2. Similarly, the value $\Delta_f H^0 = -1825.8 \pm 7.4 \text{kJ}\cdot\text{mol}^{-1}$ given in Table 3, corresponding to the value $\Delta_f G^0 = -1632.2 \pm 7.4 \text{kJ}\cdot\text{mol}^{-1}$ measured experimentally by Gorman-Lewis et al.,⁶⁵ was calculated from this $\Delta_f G^0$ value and the experimental value of the standard state entropy of metaschoepite. While the value obtained, $\Delta_f H^0 = -1825.8 \pm 7.4 \text{kJ}\cdot\text{mol}^{-1}$, is similar to that reported in most of the other experimental works, it is inconsistent with the standard state EOF measured by Kubatko et al.⁶⁴ Therefore, it is not possible that the values measured by Kubatko et al.⁶⁴ and Gorman-Lewis et al.⁶⁵ for the standard state EOF and GFEOf of metaschoepite be simultaneously correct. This would imply a value for the standard state entropy of formation of the order of $\Delta_f S^0 = 532.6 \text{kJ}\cdot\text{mol}^{-1}$, and a metaschoepite standard state entropy of about $S^0 = 293 \text{J}\cdot\text{K}^{-1}\cdot\text{mol}^{-1}$, which is higher than the value measured by Tasker et al.⁵⁶ by more than $100 \text{J}\cdot\text{K}^{-1}\cdot\text{mol}^{-1}$. The theoretical calculations for metaschoepite confirm that its standard state entropy must be much smaller than $200 \text{J}\cdot\text{K}^{-1}\cdot\text{mol}^{-1}$. Our calculated value at 298.15 K is $S = -166.24 \text{J}\cdot\text{K}^{-1}\cdot\text{mol}^{-1}$ (see Table 1). Based on this discussion, the experimental value of Kubatko et al.⁶⁴ of the EOF of metaschoepite was not used. Instead, the value used was that

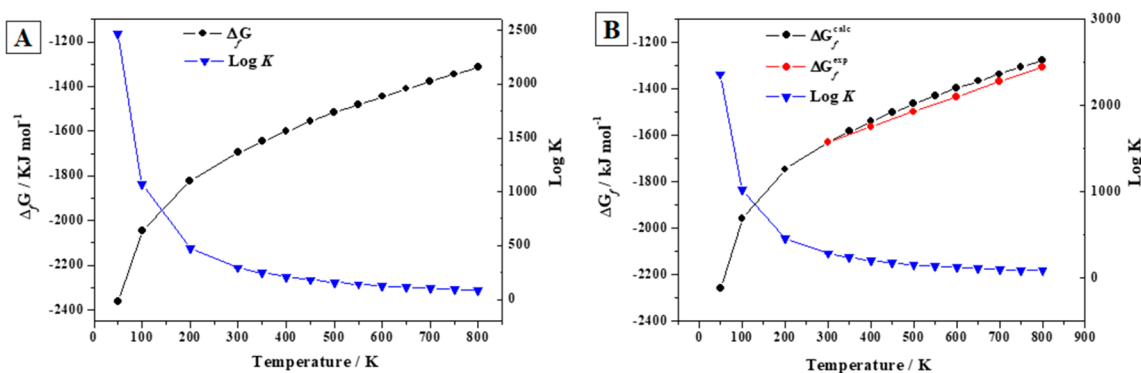


Figure 3. Calculated GFEOfs in terms of the elements and associated RCs of (A) schoepite and (B) metaschoepite as a function of temperature. The calculated GFEOfs of metaschoepite are compared with the experimental values reported by Barin.⁵⁵

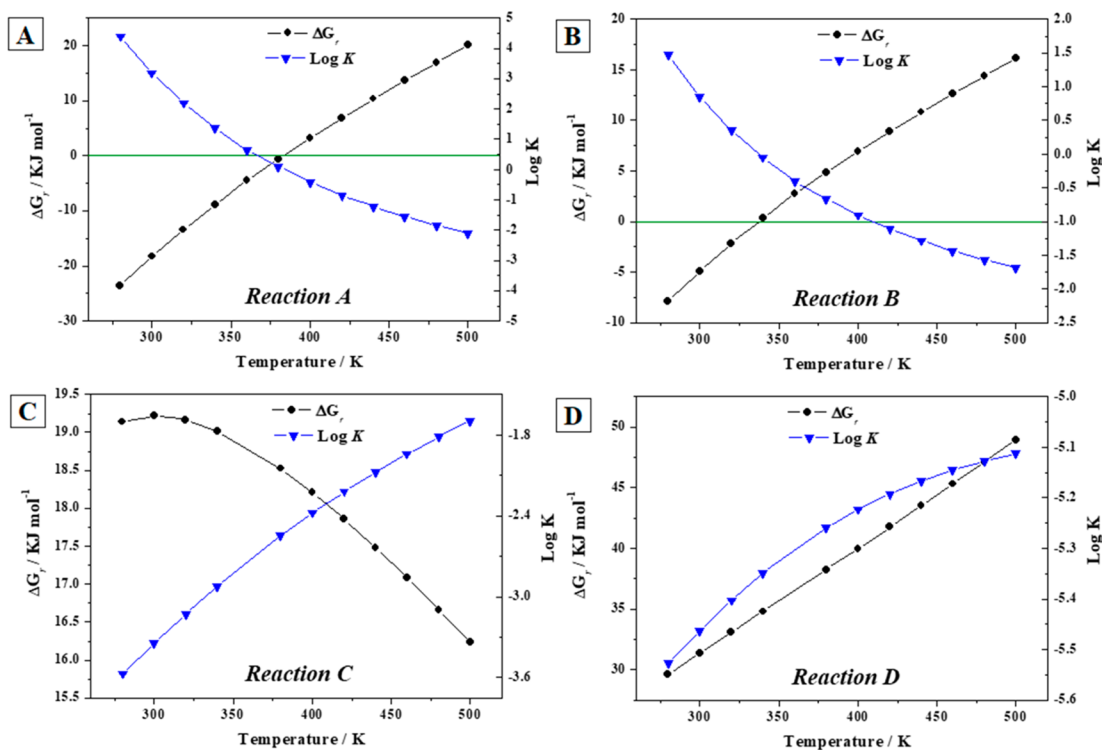


Figure 4. Calculated GFEORs and associated RCs of reactions (A) to (D) as a function of temperature.

reported by Barin,⁵⁵ $\Delta_f H^0 = -1826.70 \pm 1.0 \text{ kJ}\cdot\text{mol}^{-1}$. This value is very close to the experimental values reported by Cordfunke,⁶⁷ Hemingway,⁵⁹ and Tasker et al.⁵⁶ and to the value evaluated from the measured value of the Gibbs free energy of Gorman-Lewis et al.⁶⁵ An error of $\pm 1.0 \text{ kJ}\cdot\text{mol}^{-1}$ was included in order to estimate the influence of variations in $\Delta_f H^0$ in metaschoepite dehydration temperature.

The estimated value⁶⁰ of $\Delta_f H^0 = -1910.05 \pm 5 \text{ kJ}\cdot\text{mol}^{-1}$ for schoepite and the experimental value $\Delta_f H^0 = -1826.1 \pm 1.7 \text{ kJ}\cdot\text{mol}^{-1}$ for metaschoepite⁵⁵ were used in order to obtain the temperature dependence of their GFEOfs in terms of the elements and corresponding reaction constants in the Sections III.2.b and III.2.c. Additionally, these GFEOf values were used, in turn, in Section III.3, to obtain the GFEORs and associated temperature dependence of a series of reactions involving schoepite and metaschoepite and other UCMs, which are among the most important secondary phases appearing in the surface of the SNF under FGD conditions and, in Section III.4, to evaluate its TS with respect to these

phases. In the case that the standard state EOF of schoepite is accurately measured experimentally in the future, the corresponding temperature-dependent GFEOf of formation may be obtained by subtracting the value used for $\Delta_f H^0$ and adding the new value to the results reported in Table S.13 of the Supporting Information (see next section III.2.b).

III.2.b. EOF and GFEOf of Schoepite. By using the computed values of the TPs of schoepite, the GFEOf at the standard state reported by Finch⁶⁰ and the experimental values of the experimental TPs of the elements,^{54,55} we obtained the EOFs and GFEOfs and the associated RCs of schoepite as a function of temperature, reported in Table S.13 of the Supporting Information and displayed in Figure 3.

III.2.c. EOF and GFEOf of Metaschoepite. From the computed values of the TPs of schoepite, the experimental EOF at the standard state reported by Barin,⁵⁵ and the experimental values of the experimental TPs of the elements,^{54,55} we obtained the EOF and GFEOf functions of metaschoepite and the corresponding RCs, which are given

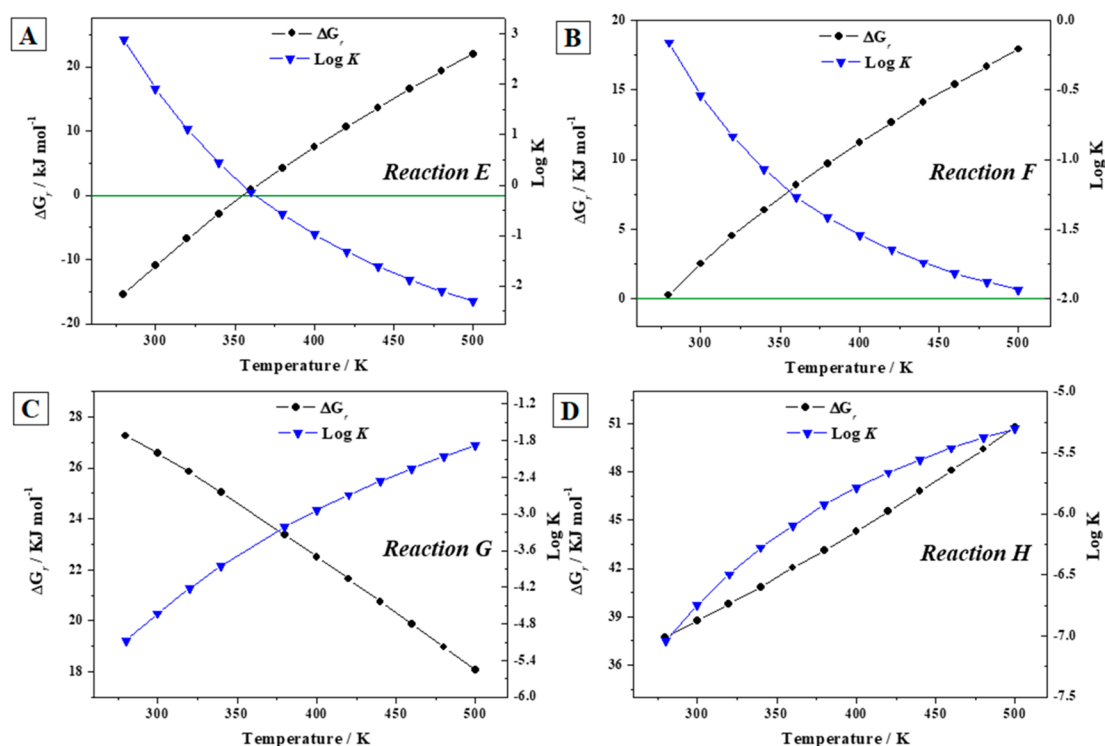


Figure 5. Calculated GFEORs and associated RCs of reactions (E) to (H) (panels A–D, respectively) as a function of temperature.

in Table S.13 of the [Supporting Information](#) and shown in [Figure 3](#). In [Table S.13](#) and [Figure 3B](#), the calculated results for metaschoepite are compared with the experimental values reported by Barin.⁵⁵ As may be seen the agreement of the theoretical and experimental data is excellent even at high temperatures. The calculated and experimental values at 800 K differ by only 2.0%. However, the calculated results cover a much larger range of temperatures from 0 to 1000 K.

III.3. Thermodynamic Properties of Reaction as a Function of Temperature. *III.3.a. EORs and GFEORs of Reactions (A) to (D).* The calculated TPFs of schoepite, given in [Section III.2.b](#), were combined with those of other important UCMs (γ - UO_3 , rutherfordine, dehydrated schoepite, and soddyite) reported in the previous work²⁹ to study the reactions (A) to (D) of the [Introduction Section](#) involving schoepite and these materials. These reactions represent the formation of schoepite in terms of the oxides and the transformations of dehydrated schoepite, rutherfordine, and soddyite minerals into schoepite, respectively. The methods and the experimental data used in order to determine the EORs and GFEORs, and associated RCs of these reactions were described in [Section II.3](#). The results are given in [Table S.14 \(Supporting Information\)](#) and displayed in [Figure 4](#).

As can be seen in [Figure 4A](#), schoepite mineral becomes unstable with respect to the corresponding oxides at a temperature of 383 ± 27 K. The error estimate in this temperature is due to the error margin in the estimate of the standard state EOF of schoepite mineral, -1910.05 ± 5.0 (see [Section III.2.a](#)). Similarly, as can be appreciated in [Figure 4B](#), the temperature of dehydration of schoepite mineral into dehydrated schoepite is 337 ± 44 K. The error estimates for the temperatures at which these two changes of the stability of schoepite are found were of the same order as those found in our previous work.³⁰

Finally, as shown in [Figure 4C,D](#), the GFEORs of reactions (D) and (E) are positive within the entire range of temperatures considered (from 280 to 500 K), and therefore, both rutherfordine and soddyite do not transform into schoepite under normal (H_2O_2 free) conditions.

III.3.b. EORs and GFEORs of Reactions (E) to (H). As in the previous section, the calculated TPFs of metaschoepite, given in [Section III.2.c](#), were combined with those of uranium trioxide, dehydrated schoepite, rutherfordine and soddyite²⁹ to study the reactions (E) to (H) of the [Introduction Section](#). These reactions represent the formation of metaschoepite in terms of the oxides and the transformations of dehydrated schoepite, rutherfordine, and soddyite minerals into metaschoepite, respectively. The results are given in [Table S.15](#) of the [Supporting Information](#) and displayed in [Figure 5](#).

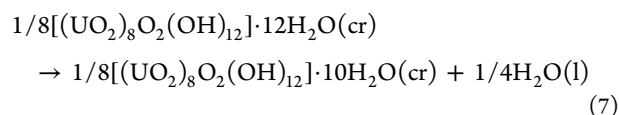
[Figure 5A](#) shows that metaschoepite becomes unstable with respect to the corresponding oxides at a temperature 355 ± 6 K. Similarly, as can be appreciated in [Figure 5B](#), the temperature of dehydration of metaschoepite mineral into dehydrated schoepite is 278 ± 9 K.

As shown below, at H_2O_2 free conditions, schoepite has a TS that is very similar to that of metaschoepite (see [Section III.3.c](#) for the precise values of the EOR and GFEOR values for the corresponding dehydration reaction). Schoepite is shown to be only slightly more stable than metaschoepite. This was expected since the distinction between schoepite and metaschoepite both at laboratory and natural settings is complicated, and the samples usually involve a mixture of both phases.

Heating schoepite, metaschoepite, and dehydrated schoepite ($\text{UO}_3 \cdot x\text{H}_2\text{O}$; $0.75 < x < 1$) are formed by a stepwise loss of water. The TGA studies of Dawson et al.⁷⁰ showed that metaschoepite loses water in two stages, being converted into $\text{UO}_3 \cdot 0.80 \text{H}_2\text{O}$ between 293 and 413 K and into UO_3 at 633 K. The DTA and TGA measurements of Lindval and

Kuznetsova^{71,61} showed that, in fact, the initial decomposition product is $\text{UO}_3 \cdot 0.75 \text{H}_2\text{O}$ and that subsequent heating leads to the formation of UO_3 and finally to U_3O_8 . The TGA results of Perez-Bustamante et al.^{72,61} showed that $\text{UO}_3 \cdot 0.75 \text{H}_2\text{O}$ was formed up to 452 K. Most of these observations have been confirmed by several studies as those of Hoekstra and Siegel.⁷³ Our results show that metaschoepite decomposes into UO_3 from 355 K since the GFEOR of reaction (E) becomes positive at this temperature. However, according to reaction (F) metaschoepite converts into dehydrated schoepite ($\text{UO}_3 \cdot 1 \text{H}_2\text{O}$) at 278 K. Since dehydrated schoepite is more stable than UO_3 ³⁰ and dehydrates to UO_3 at about 463 K, metaschoepite must dehydrate first at 278 K becoming dehydrated schoepite, and then, this compound dehydrates to UO_3 at about 463 K. This final temperature of dehydration to UO_3 is in very good agreement with the experimental value of 452 K. According to our previous work,³⁰ further heating leads to U_3O_8 , the transformation beginning at a temperature of 488 K. The conversion rate reaches a maximum at about 759 K.

III.3.c. Thermodynamics of the Reaction of Dehydration of Schoepite into Metaschoepite. The reaction of dehydration of schoepite into metaschoepite may be written as



The calculated TPFs of schoepite and metaschoepite, given in Sections III.2.b and III.2.c, were combined with the experimental ones of H_2O from JANAF tables⁵⁴ to study this dehydration reaction. The results are given in Table S.17 of the Supporting Information and displayed in Figure 6. As was

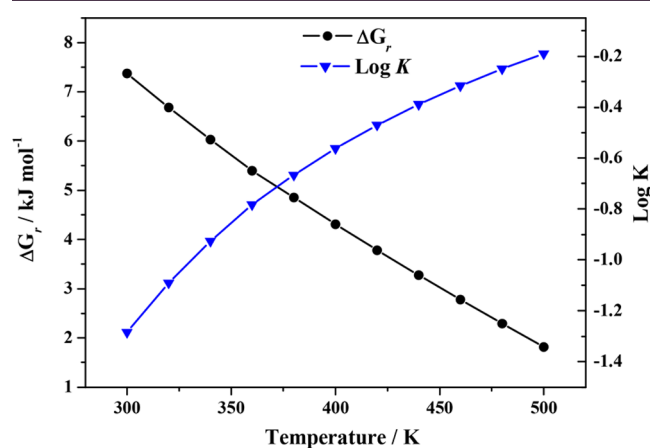


Figure 6. Calculated GFEORs of the reaction 7 of dehydration of schoepite into metaschoepite.

already mentioned in the previous section, schoepite has a TS that is very similar to that of metaschoepite at H_2O_2 free conditions. Schoepite is found to be only slightly more stable than metaschoepite.

III.3.d. EORs and GFEORs of Reactions (I) to (L). The calculated TPFs of schoepite and metaschoepite were combined with those of metastudtite and studtite reported in our previous work²⁹ to study the reactions (I) to (L) of the Introduction Section. Reactions (I) and (J) represent the transformation of schoepite into metastudtite and studtite in the presence of water and H_2O_2 and in the presence of H_2O_2 and absence of water, respectively. Reactions (K) and (L)

represent the transformations of metaschoepite into schoepite under the same conditions. The last situation is very important since it is the one expected under high radiation fields, which cause the radiolysis of the water reaching the surface of the SNF. The experimental data used in order to determine the EORS and GFEORs and associated RCs of these reactions were described in Section II.3. The results are given in Table S.16 (see Supporting Information) and displayed in Figure 7.

Since the GFEORs of reaction (1) are positive everywhere (see Figure 7A), schoepite will not transform spontaneously into metastudtite in the presence of water and H_2O_2 . Therefore, schoepite is highly stabilized under the presence of water and H_2O_2 , becoming more stable than metastudtite. The opposite behavior is observed for reaction (J). In this case the GFEORs are negative within the full range of temperature considered (see Figure 7B), and consequently, schoepite will be converted into studtite under high H_2O_2 concentrations. This means that the stabilization of schoepite is not as large as that of studtite phase, which, as shown in the next section, is the most stable secondary phase of the spent nuclear fuel at these conditions among those considered in this work. Because the GFEORs of reactions (K) and (L) are positive everywhere (see Figures 7C and 7D), metaschoepite is less stable than schoepite not only under H_2O_2 free conditions but also under the presence of H_2O_2 . In fact, the difference in the stabilities of these phases increases as the amount of H_2O_2 increases. At 298 K, the free energies of the transformation of schoepite into metaschoepite increases from 8.0 kJ·mol⁻¹ at H_2O_2 free conditions to 37.2 kJ·mol⁻¹ at high H_2O_2 conditions (see Table S.16 and S.17 in the Supporting Information).

Dehydrated schoepite and soddyite readily transform into studtite under high H_2O_2 concentrations as shown by Forbes et al.⁷⁴ Similarly, Kubatko et al.⁷⁵ showed that becquerelite transforms completely into studtite in the presence of high concentrations of H_2O_2 in only 8 h. The transformation of uranium trioxide, rutherfordine, and metastudtite into studtite was also predicted in our previous work.³⁰ The same should also occur for schoepite and metaschoepite.

III.4. Relative TS of Schoepite with Respect to Other Secondary Phases of the SNF. Using the results obtained in this Article and those reported previously,³⁰ the order of stability of schoepite, metaschoepite, dehydrated schoepite, studtite, metastudtite, soddyite, rutherfordine, and $\gamma\text{-UO}_3$ may be evaluated: (A) in the absence of H_2O_2 ; (B) in the presence of water and H_2O_2 ; and (C) in the presence of high H_2O_2 concentrations. The relative TS of these phases at these conditions is displayed in Figure 8. In Figures 8A–C, the relative TSs are measured with respect to $\gamma\text{-UO}_3$, metastudtite, and studtite, respectively.

As shown in Figure 8A, in the absence of H_2O_2 , soddyite is the most stable phase and rutherfordine is also more stable than schoepite and metaschoepite. Thus, at H_2O_2 free conditions, in the presence of silicate or carbonate ions, schoepite and metaschoepite should be replaced by other mineral phases. In the presence of water and H_2O_2 , as shown in Figure 8B, schoepite and metaschoepite are very highly stabilized and become the first and second most stable phases, respectively. Finally, as can be seen in Figure 8C, and it also occurs to studtite phase,³⁰ the TS of these phases also increases under high H_2O_2 concentrations. However, the stabilization of schoepite and metaschoepite is not as large as that of the studtite phase, and they become the second and third most stable phases at these conditions among those considered in

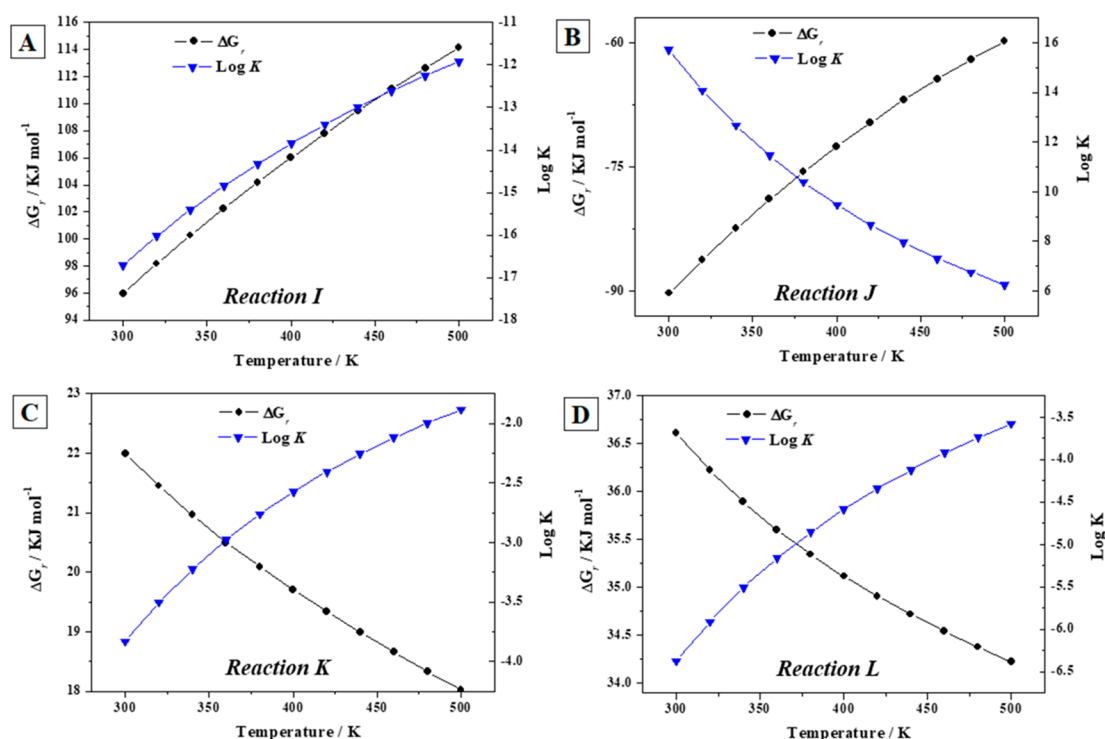
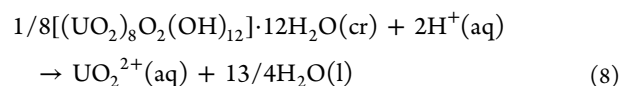


Figure 7. Calculated GFEORs and associated RCs of reactions (I) to (L) (panels A–D), respectively) as a function of temperature.

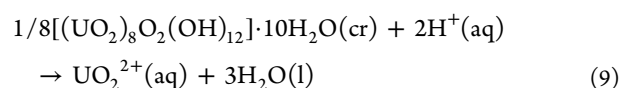
this work. Schoepite phase is less stable than studtite by about 90 and 60 $\text{kJ}\cdot\text{mol}^{-1}$ at 298.15 and 500 K, respectively, and more stable than metastudtite by about 230 and 207 $\text{kJ}\cdot\text{mol}^{-1}$ at 298.15 and 500 K, respectively.

Studtite TS decreases largely with the decrease of H_2O_2 concentration and the increase of temperature. When the concentration of H_2O_2 diminishes with time, as expected from the decrease of the intensity of radiation fields over time in a RNWR,⁷⁶ the stability of this hydrated uranyl peroxide phase will decrease, and other secondary phases will be formed. However, in order to evaluate the TS of the secondary phases of the SNF in a precise way, an extended study must be carried out including a more significant number of secondary phases. The full evaluation of the relative amounts of secondary phases of SNF at FGD conditions over time requires the realization of complete thermodynamic calculations using thermochemical data for an appreciable number of materials including aqueous species, the most important secondary phases, and amorphous phases at different temperature and pressure conditions.³⁰

III.5. Solubility Reaction Constants of Schoepite and Metaschoepite. The solubility reactions of schoepite and metaschoepite are, respectively



and



Using the computed values of the GFEOR of schoepite and metaschoepite and the GFEOR of aqueous uranyl ion, $\text{UO}_2^{2+}(\text{aq})$, and water at 298.15 K,⁷⁷ one obtains the GFEORs and associated RCs of reactions 8 and 9 given in Table 4. As

can be seen, the calculated solubility product of metaschoepite, $\log K_{\text{sp}}^{\text{calc}} = 5.98$, is in excellent agreement with the experimental value reported by Gorman-Lewis et al.⁶⁵ ($\log K_{\text{sp}}^{\text{exp}} = 5.60 \pm 0.2$). Schoepite is shown to be more insoluble than metaschoepite.

IV. CONCLUSIONS

The TPs of schoepite and metaschoepite minerals were determined by using theoretical solid-state methods based on density functional theory using plane waves and pseudopotentials. Since these properties have not been measured experimentally for schoepite, their values were predicted. The results obtained of metaschoepite were found to be in very good agreement with the experimental values from Barin.⁵⁵ The calculated TPs of these materials were used in order to obtain their EOF and GFEOR as a function of temperature. The calculated GFEORs of metaschoepite are in excellent agreement with the experimental data even at high temperatures.⁵⁵ Then, these TPs were combined with those of other important UCMs (rutherfordine, γ -uranium trioxide, dehydrated schoepite, and soddyite) to study eight reactions involving schoepite and metaschoepite and these materials. The results showed that schoepite becomes unstable with respect to the corresponding oxides at temperatures higher than 110 °C (383 ± 27 K) and that the dehydration of schoepite occurs at 64 °C (337 ± 44 K). The corresponding values of these temperatures for metaschoepite are 79 °C (355 ± 6 K) and 5 °C (278 ± 9 K), respectively. Under H_2O_2 free conditions and within the full range of temperatures considered, from 280 to 500 K, schoepite is less stable than rutherfordine and soddyite.

The relative TS of schoepite with respect to the uranyl peroxide hydrates metastudtite and studtite was studied under different conditions of temperature and concentrations of H_2O_2 by considering the corresponding reactions. Besides, the

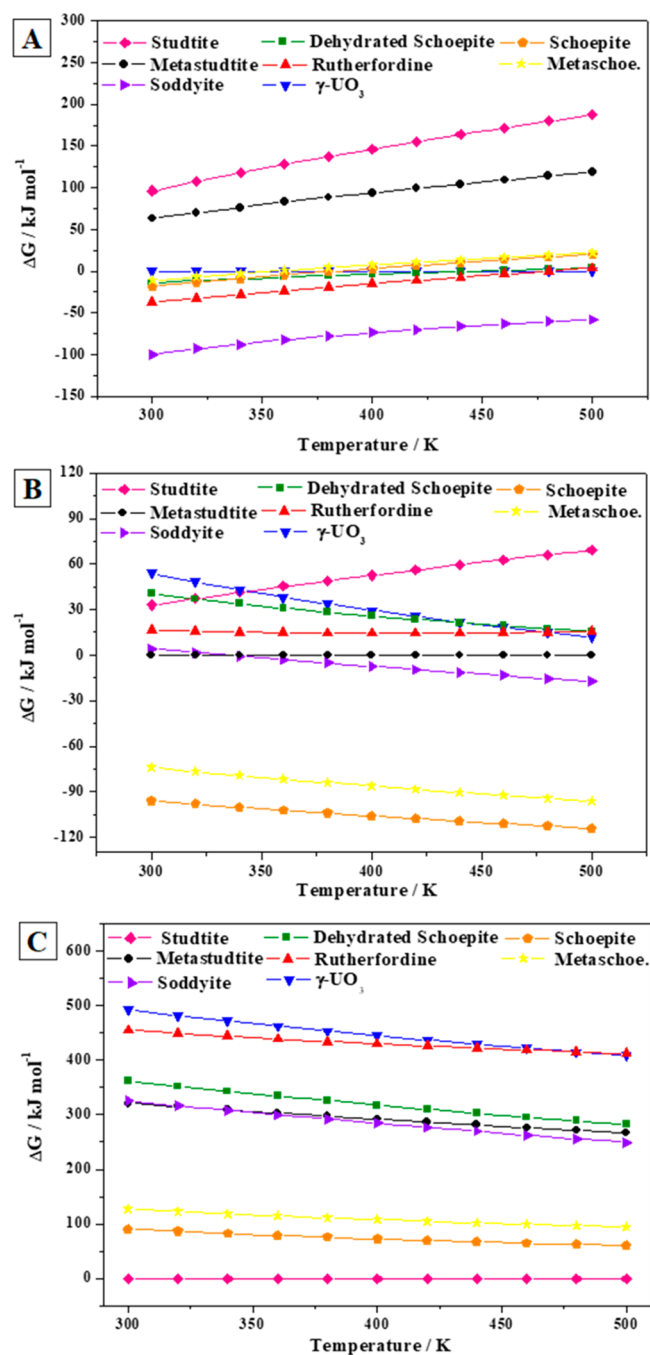


Figure 8. Relative TS of schoepite and metaschoepite with respect to other secondary phases of SNF: (A) under the absence of H_2O_2 ; (B) under the presence of water and H_2O_2 ; and (C) under high concentrations of H_2O_2 .

Table 4. Calculated GFEORs ($\Delta_r G$) and Associated RCs ($\log K$) of the Reactions of Solubility of Schoepite and Metaschoepite (Reactions 8 and 9, respectively)^a

mineral	$\Delta_r G^{\text{calc}}$	$\log K_{\text{sp}}^{\text{calc}}$	$\log K_{\text{sp}}^{\text{exp}}$ (ref 65)
schoepite	-26.11	4.57	
metaschoepite	-34.14	5.98	5.60 ± 0.2

^aThe values of $\Delta_r G$ are in units of $\text{kJ}\cdot\text{mol}^{-1}$.

relative stability of metaschoepite with respect to schoepite at these conditions was evaluated from the TPs of the corresponding transformation reactions. Schoepite and meta-

schoepite are shown to have very similar TSs, the first being slightly more stable than the second one. From these computations, we have been able to determine the EORs and GFEORs and the associated RCs of these reactions for a wide range of temperatures. These results obtained in this work allowed to determine the relative TS of schoepite and metaschoepite with respect to a series of the most important SNF secondary phases under different conditions. These results show that, among the mineral phases considered in this study, schoepite and metaschoepite are the first and second most stable phases under intermediate H_2O_2 concentrations. Besides, they are, after studtite, the second and third most stable phases under high H_2O_2 concentrations. This situation is important since it is the one expected under high radiation fields producing the radiolysis of water on the surface of the spent nuclear fuel. Finally, the solubility reaction constants of schoepite and metaschoepite were determined. The calculated solubility product of metaschoepite was in excellent agreement with the experimental value. Schoepite is shown to be more insoluble than metaschoepite.

■ ASSOCIATED CONTENT

📄 Supporting Information

The Supporting Information is available free of charge on the ACS Publications website at DOI: 10.1021/acsearthspacechem.8b00109.

Calculated TPs of schoepite and metaschoepite in the temperature range from 0 to 1000 K. Comparison of the calculated and experimental TPs of schoepite and metaschoepite in the temperature range from 0 to 360 K and 298.15 to 800 K. Calculated EOFs and GFEORs and associated RCs of schoepite and metaschoepite. Calculated EORs and GFEORs of the reactions (A)–(D), (E)–(H), (I)–(L), and the reaction of dehydration of schoepite into metaschoepite. Theoretical solid-state calculations of the crystal structure and X-ray powder diffraction pattern of metaschoepite mineral (PDF)

Computed crystal structure of metaschoepite (CIF)

■ AUTHOR INFORMATION

Corresponding Author

*E-mail: francisco.colmenero@iem.cfmac.csic.es. Phone: +34 915616800, ext. 941033.

ORCID

Francisco Colmenero: 0000-0003-3418-0735

Notes

The authors declare no competing financial interest.

■ ACKNOWLEDGMENTS

This work has been carried out in the context of the ENRESÁS project: N° 079000189 “Aplicación de técnicas de caracterización en el estudio de la estabilidad del combustible nuclear irradiado en condiciones de almacenamiento” (ACESCO) under a CSIC–CIEMAT collaboration agreement: “Caracterización experimental y teórica de fases secundarias y óxidos de uranio formados en condiciones de almacenamiento de combustible nuclear”. CETA-CIEMAT, CTI-CSIC, and CESGA centers are acknowledged for the used supercomputer time.

REFERENCES

- (1) Walker, T. L. Schoepite a New Uranium Mineral from Kasolo, Belgian Congo. *Am. Mineral.* **1923**, *8*, 67–69.
- (2) Schoep, A. The Specific Gravity and Chemical Composition of Becquerelite and Schoepite. *Ann. Mus. Congo Belge. (Mineralogie)* **1932**, *1*, Fasc. III, 5–7.
- (3) Billiet, V.; De Jong, W. F. Schoepiet en Becquereliet. *Naturw. Tijdschr. Ned-Ind.* **1935**, *17*, 157–162.
- (4) Schoep, A.; Stradiot, S. Paraschoepite and Epianthinite, Two New Uranium Minerals from Shinkolobwe (Belgian Congo). *Am. Mineral.* **1947**, *32*, 344–350.
- (5) Christ, C. L.; Clark, J. R. Crystal Chemical Studies of Some Uranyl Oxide Hydrates. *Am. Mineral.* **1960**, *45*, 1026–1061.
- (6) Finch, R. J.; Cooper, M. A.; Hawthorne, F. C.; Ewing, R. C. The Crystal Structure of Schoepite, $[(\text{UO}_2)_8\text{O}_2(\text{OH})_{12}](\text{H}_2\text{O})_{12}$. *Can. Mineral.* **1996**, *34*, 1071–1088.
- (7) Finch, R. J.; Hawthorne, F. C.; Miller, M. L.; Ewing, R. C. Distinguishing Among Schoepite, $[(\text{UO}_2)_8\text{O}_2(\text{OH})_{12}](\text{H}_2\text{O})_{12}$, and Related Minerals by X-Ray Powder Diffraction. *Powder Diffr.* **1997**, *12*, 230–238.
- (8) Sowder, A. G.; Clark, S. B.; Fjeld, R. A. The Transformation of Uranyl Oxide Hydrates: The Effect of Dehydration on Synthetic Metaschoepite and Its Alteration to Becquerelite. *Environ. Sci. Technol.* **1999**, *33*, 3552–3557.
- (9) Weller, M. T.; Light, M. E.; Gelbrich, T. Structure of Uranium(VI) Oxide Dihydrate, $\text{UO}_3 \cdot 2\text{H}_2\text{O}$; Synthetic Meta-Schoepite $(\text{UO}_2)_4\text{O}(\text{OH})_6 \cdot 5\text{H}_2\text{O}$. *Acta Crystallogr., Sect. B: Struct. Sci.* **2000**, *56*, 577–583.
- (10) Plasil, J. Oxidation-Hydration Weathering of Uraninite: The Current State-of Knowledge. *J. Geosci.* **2014**, *59*, 99–114.
- (11) Frondel, C. Mineral Composition of Gummite. *Am. Mineral.* **1956**, *41*, 539–568.
- (12) Finch, R. J.; Ewing, R. C. The Corrosion of Uraninite under Oxidizing Conditions. *J. Nucl. Mater.* **1992**, *190*, 133–156.
- (13) Finch, R. J.; Miller, M. L.; Ewing, R. C. Weathering of Natural Oxide Hydrates: Schoepite Polytypes and Dehydration Effects. *Radiochim. Acta* **1992**, *58/59*, 433–443.
- (14) Grenthe, I.; Drozdzyński, J.; Fujino, T.; Buck, E. C.; Albrecht-Schmitt, T. E.; Wolf, S. F. Uranium. In *The Chemistry of Actinide and Transactinide Elements*; Morss, L. R., Edelstein, N. M., Fuger, J., Eds.; Springer Science and Business Media: Berlin, 2006; Vol. I, Chapter V, pp 253–638.
- (15) Percy, E. C.; Prikryl, J. D.; Murphy, W. M.; Leslie, B. W. Alteration of Uraninite from the Nopal I Deposit, Peña Blanca District, Chihuahua, Mexico, Compared to Degradation of Spent Nuclear Fuel in the Proposed US High-Level Nuclear Waste Repository at Yucca Mountain, Nevada. *Appl. Geochem.* **1994**, *9*, 713–732.
- (16) Wronkiewicz, D. J.; Bates, J. K.; Gerding, T. J.; Veleckis, E.; Tani, B. S. Uranium Release and Secondary Phase Formation During Unsaturated Testing of UO_2 at 90°C. *J. Nucl. Mater.* **1992**, *190*, 107–127.
- (17) Wronkiewicz, D. J.; Bates, J. K.; Wolf, S. F.; Buck, E. C. Ten-Year Results from Unsaturated Drip Tests with UO_2 at 90°C: Implications for the Corrosion of Spent Nuclear Fuel. *J. Nucl. Mater.* **1996**, *238*, 78–95.
- (18) Christensen, H.; Sunder, S. An evaluation of water layer thickness effective in the oxidation of UO_2 fuel due to radiolysis of water. *J. Nucl. Mater.* **1996**, *238*, 70–77.
- (19) Shoosmith, D. W. Fuel corrosion processes under waste disposal conditions. *J. Nucl. Mater.* **2000**, *282*, 1–31.
- (20) Sunder, S. Calculation of radiation dose rates in a water layer in contact with used CANDU UO_2 fuel. *Nucl. Technol.* **1998**, *122*, 211–221.
- (21) Wang, R.; Katayama, Y. B. Dissolution mechanisms for UO_2 and spent fuel. *Nucl. Chem. Waste Manage.* **1982**, *3*, 83–90.
- (22) Sattonnay, G.; Ardois, C.; Corbel, C.; Lucchini, J. F.; Barthe, M. F.; Garrido, F.; Gosset, D. Alpha-radiolysis effects on UO_2 alteration in water. *J. Nucl. Mater.* **2001**, *288*, 11–19.
- (23) Amme, M.; Renker, B.; Schmid, B.; Feth, M. P.; Bertagnolli, H.; Döbelin, W. Raman microspectrometric identification of corrosion products formed on UO_2 nuclear fuel during leaching experiments. *J. Nucl. Mater.* **2002**, *306*, 202–212.
- (24) Burakov, B. E.; Strykanova, E. E.; Anderson, E. B. Secondary Uranium Minerals on the Surface of Chernobyl “lava. *MRS Online Proc. Libr.* **1996**, *465*, 1309–1311.
- (25) Abrefah, J.; Marschmann, S.; Jensen, E. D. *Examination of the Surface Coatings Removed from K-East Basin Fuel Elements*; Report of the U.S. Department of Energy, Pacific Northwest National Laboratory PNNL-11806; US-DOE: Richland, WA, 1998.
- (26) Schmidt, A. J.; Delegard, C. H. *Assessment of K Basin Sludge Vol. Expansion Resulting from Uranium Corrosion During Storage*; Report of the U.S. Department of Energy, Pacific Northwest National Laboratory PNNL-13786; US-DOE: Richland, WA, 2002.
- (27) Delegard, C. H.; Schmidt, A. J. *Uranium Metal Reaction Behavior in Water, Sludge, and Grout*; Report of the U.S. Department of Energy, Pacific Northwest National Laboratory PNNL-17815; US-DOE: Richland, WA, 2008.
- (28) Payne, M. C.; Teter, M. P.; Ailan, D. C.; Arias, A.; Joannopoulos, J. D. Iterative Minimization Techniques for *Ab Initio* Total-Energy Calculations: Molecular Dynamics and Conjugate Gradients. *Rev. Mod. Phys.* **1992**, *64*, 1045–1097.
- (29) Colmenero, F.; Fernández, A. M.; Cobos, J.; Timón, V. Thermodynamic Properties of Uranyl Containing Materials Based on Density Functional Theory. *J. Phys. Chem. C* **2018**, *122*, 5254–5267.
- (30) Colmenero, F.; Fernández, A. M.; Cobos, J.; Timón, V. Temperature Dependent Free Energies of Reaction of Uranyl Containing Materials Based on Density Functional Theory. *J. Phys. Chem. C* **2018**, *122*, 5268–5279.
- (31) Clark, S. J.; Segall, M. D.; Pickard, C. J.; Hasnip, P. J.; Probert, M. I. J.; Refson, K.; Payne, M. C. First Principles Methods Using CASTEP. *Z. Kristallogr. - Cryst. Mater.* **2005**, *220*, 567–570. Milman, V.; Refson, K.; Clark, S. J.; Pickard, C. J.; Yates, J. R.; Gao, S. P.; Hasnip, P. J.; Probert, M. I. J.; Perlov, A.; Segall, M. D. Electron and Vibrational Spectroscopies Using DFT, Plane Waves and Pseudopotentials: CASTEP Implementation. *J. Mol. Struct.: THEOCHEM* **2010**, *954*, 22–35.
- (32) MaterialsStudio. <http://3dsbiovia.com/products/collaborative-science/biovia-materials-studio/>, accessed September 27, 2018.
- (33) Grimme, S. Semiempirical GGA-type Density Functional Constructed with a Long-Range Dispersion Correction. *J. Comput. Chem.* **2006**, *27*, 1787–1799.
- (34) Perdew, J. P.; Burke, K.; Ernzerhof, M. Generalized Gradient Approximation Made Simple. *Phys. Rev. Lett.* **1996**, *77*, 3865–3868.
- (35) Troullier, N.; Martins, J. L. Efficient Pseudopotentials for Plane-Wave Calculations. *Phys. Rev. B: Condens. Matter Mater. Phys.* **1991**, *43*, 1993–2006.
- (36) Bonales, L. J.; Colmenero, F.; Cobos, J.; Timón, V. Spectroscopic Raman Characterization of Rutherfordine: a Combined DFT and Experimental Study. *Phys. Chem. Chem. Phys.* **2016**, *18*, 16575–16584.
- (37) Colmenero, F. *Characterization of Secondary Phases of Spent Nuclear Fuel under Final Geological Disposal Conditions*. Ph.D. Thesis. Universidad Autónoma de Madrid, Madrid, 2017.
- (38) Colmenero, F.; Bonales, L. J.; Cobos, J.; Timón, V. Study of the Thermal Stability of Studtite by *In Situ* Raman Spectroscopy and DFT Calculations. *Spectrochim. Acta, Part A* **2017**, *174*, 245–253.
- (39) Colmenero, F.; Bonales, L. J.; Cobos, J.; Timón, V. Structural, Mechanical and Vibrational Study of Uranyl Silicate Mineral Sodydite by DFT Calculations. *J. Solid State Chem.* **2017**, *253*, 249–257.
- (40) Colmenero, F.; Bonales, L. J.; Cobos, J.; Timón, V. Thermodynamic and Mechanical Properties of Rutherfordine Mineral Based on Density Functional Theory. *J. Phys. Chem. C* **2017**, *121*, 5994–6001.
- (41) Colmenero, F.; Bonales, L. J.; Cobos, J.; Timón, V. Density Functional Theory Study of the Thermodynamic and Raman Vibrational Properties of γ - UO_3 Polymorph. *J. Phys. Chem. C* **2017**, *121*, 14507–14516.

- (42) Colmenero, F.; Bonales, L. J.; Cobos, J.; Timón, V. Structural, Mechanical and Raman Spectroscopic Characterization of Layered Uranyl Silicate Mineral Uranophane- α by DFT Methods. *Clay Miner.* **2018**, *53*.
- (43) Colmenero, F.; Cobos, J.; Timón, V. Periodic DFT Study of the Structure, Raman Spectrum and Mechanical Properties of Schoepite Mineral. *Inorg. Chem.* **2018**, *57*, 4470–4481.
- (44) Weck, P. F.; Kim, E. Layered Uranium(VI) Hydroxides: Structural and Thermodynamic Properties of Dehydrated Schoepite α - $\text{UO}_2(\text{OH})_2$. *Dalton Trans* **2014**, *43*, 17191–17199.
- (45) Weck, P. F.; Kim, E. Uncloaking the Thermodynamics of the Studtite to Metastudtite Shear-Induced Transformation. *J. Phys. Chem. C* **2016**, *120*, 16553–16560.
- (46) Sassani, D. C.; Jové-Colón, C. F.; Weck, P. F.; Jerden, J. L.; Frey, K. E.; Cruse, T.; Ebert, W. L.; Buck, E. C.; Wittman, R. S. *Used Fuel Degradation: Experimental and Modeling Report, Fuel Cycle Research and Development Report FCRD-UFD-2013-000404*; Sandia National Laboratories: Albuquerque, NM, October 17, 2013.
- (47) Beridze, G.; Kowalski, P. M. Benchmarking the DFT+U Method for Thermochemical Calculations of Uranium Molecular Compounds and Solids. *J. Phys. Chem. A* **2014**, *118*, 11797–11810.
- (48) Baroni, S.; de Gironcoli, S.; Dal Corso, A. Phonons and Related Crystal Properties from Density-Functional Perturbation Theory. *Rev. Mod. Phys.* **2001**, *73*, 515–562.
- (49) Baroni, S.; Giannozzi, P.; Testa, A. Green's-Function Approach to Linear Response in Solids. *Phys. Rev. Lett.* **1987**, *58*, 1861–1864.
- (50) Gonze, X.; Lee, C. Dynamical Matrices, Born Effective Charges, Dielectric Permittivity Tensors, and Interatomic Force Constants from Density-Functional Perturbation Theory. *Phys. Rev. B: Condens. Matter Mater. Phys.* **1997**, *55*, 10355–10368.
- (51) Gonze, X.; Allan, D. C.; Teter, M. P. Dielectric Tensor, Effective Charges and Phonon in α -Quartz by Variational Density-Functional Perturbation Theory. *Phys. Rev. Lett.* **1992**, *68*, 3603–3606.
- (52) Refson, K.; Tulip, P. R.; Clark, S. J. Variational Density-Functional Perturbation Theory for Dielectrics and Lattice Dynamics. *Phys. Rev. B: Condens. Matter Mater. Phys.* **2006**, *73*, 155114.
- (53) Lee, C.; Gonze, X. Ab Initio Calculation of the Thermodynamic Properties and Atomic Temperature Factors of SiO_2 α -Quartz and Stishovite. *Phys. Rev. B: Condens. Matter Mater. Phys.* **1995**, *51*, 8610–8613.
- (54) Chase, M. W.; Davies, C. A.; Downey, J. R.; Frurip, D. J.; McDonald, R. A.; Syverud, A. N. JANAF Thermochemical Tables. Third Edition. *J. Phys. Chem. Ref. Data* **1985**, *14* (Suppl. 1), 1–1856.
- (55) Barin, I. *Thermochemical Data of Pure Substances*; 3rd ed.; VCH: Weinheim, 1995.
- (56) Tasker, I. R.; O'Hare, P. A. G.; Lewis, B. M.; Johnson, G. K. Thermochemistry of Uranium Compounds. XVI. Calorimetric Determination of the Standard Molar Enthalpy of Formation at 298.15 K, Low-Temperature Heat Capacity, and High-Temperature Enthalpy Increments of $\text{UO}_2(\text{OH})_2 \cdot \text{H}_2\text{O}$ (Schoepite). *Can. J. Chem.* **1988**, *66*, 620–625.
- (57) Debets, P. C.; Loopstra, B. O. On the Uranates of Ammonium. II. X-Ray Investigation of the Compounds in the System $\text{NH}_3\text{-UO}_3\text{-H}_2\text{O}$. *J. Inorg. Nucl. Chem.* **1963**, *25*, 945–953.
- (58) Langmuir, D. Uranium Solution-Mineral Equilibria at Low Temperatures with Applications to Sedimentary Ore Deposits. *Geochim. Cosmochim. Acta* **1978**, *42*, 547–569.
- (59) Hemingway, B. S. *Thermodynamic Properties of Selected Uranium Compounds and Aqueous Species at 298.15 K and 1 bar and at Higher Temperatures - Preliminary Models for the Origin of Coffinite Deposits*; USGS Open-File Report 82–619: 1982.
- (60) Finch, R. J. Thermodynamic Stabilities of U(VI) Minerals: Estimated and Observed Relationships. *MRS Online Proc. Libr.* **1996**, *465*, 1185–1192.
- (61) O'Hare, P. A. G.; Lewis, B. M.; Nguyen, S. N. Thermochemistry of Uranium Compounds XVI I. Standard Molar Enthalpy of Formation at 298.15 K of Dehydrated Schoepite $\text{UO}_2 \cdot 0.9\text{H}_2\text{O}$. Thermodynamics of (Schoepite + Dehydrated Schoepite + Water). *J. Chem. Thermodyn.* **1988**, *20*, 1287–1296.
- (62) Grenthe, I.; Fuger, J.; Konings, R. J. M.; Lemire, R. J.; Muller, A. B.; Nguyen-Trung, C.; Wanner, H. *Chemical Thermodynamics of Uranium*; Nuclear Energy Agency Organisation for Economic Co-Operation and Development, OECD: Issy-les-Moulineaux, France, 2004.
- (63) Guillaumont, N. Y. R.; Fanghänel, T.; Neck, V.; Fuger, J.; Palmer, D. A.; Grenthe, I.; Rand, M. H. *Update on the Chemical Thermodynamics of Uranium, Neptunium, Plutonium, Americium, and Technetium*; Mompean, F. J., Illemassene, M., Domenech-Orti, C., Ben Said, K., Eds.; OECD Nuclear Energy Agency, Data Bank: Issy-les-Moulineaux, France, 2003.
- (64) Kubatko, K.-A.; Helean, K.; Navrotsky, A.; Burns, P. C. Thermodynamics of Uranyl Minerals: Enthalpies of formation of Uranyl Oxide Hydrates. *Am. Mineral.* **2006**, *91*, 658–666.
- (65) Gorman-Lewis, D.; Fein, J. B.; Burns, P. C.; Szymanowski, J. E. S.; Converse, J. Solubility Measurements of the Uranyl Oxide Hydrate Phases Metaschoepite, Compreignacite, Na–Compreignacite, Becquerelite, and Clarkeite. *J. Chem. Thermodyn.* **2008**, *40*, 980–990.
- (66) Shvareva, T. Y.; Fein, J. B.; Navrotsky, A. Thermodynamic Properties of Uranyl Minerals: Constraints from Calorimetry and Solubility Measurements. *Ind. Eng. Chem. Res.* **2012**, *51*, 607–613.
- (67) Cordfunke, E. H. P. Heats of Formation of Some Hexavalent Uranium Compounds. *J. Phys. Chem.* **1964**, *68*, 3353–3356.
- (68) Clark, S. B.; Ewing, R. C.; Schaumlöffel, J. C. A Method to Predict Free Energies of Formation of Mineral Phases in the $\text{U(VI)-SiO-H}_2\text{O}$ System. *J. Alloys Compd.* **1998**, *271–273*, 189–193.
- (69) Chen, F.; Ewing, R. C.; Clark, S. B. The Gibbs Free Energies and Enthalpies of Formation of U^{6+} Phases: An Empirical Method of Prediction. *Am. Mineral.* **1999**, *84*, 650–664.
- (70) Dawson, J. K.; Wait, E.; Alcock, K.; Chilton, D. R. Some Aspects of the System Uranium Trioxide–Water. *J. Chem. Soc.* **1956**, *0*, 3531–3540.
- (71) Lindval, R. V.; Kuznetsova, V. V. Report Related to Uranium. 3. Thermophysical Study of Hydrated Uranium (VI) Oxides and Ammonium Uranates (in Russian). *Tr. Kazan. Khim. Tekhnol. Inst.* **1974**, *54*, 145–150.
- (72) Perez-Bustamante, J. A.; Polonio, J. B.; Cellini, R. F. Contribución al Estudio de los Carbonatos Complejos de Urano. I. *Anal. Real Soc. Esp. Fis. Quim.* **1962**, *B58*, 677–704.
- (73) Hoekstra, H. R.; Siegel, S. J. The Uranium Trioxide–Water System. *J. Inorg. Nucl. Chem.* **1973**, *35*, 761–779.
- (74) Forbes, T. Z.; Horan, P.; Devine, T.; McInnis, D.; Burns, P. C. Alteration of Dehydrated Schoepite and Sodydite to Studtite, $[(\text{UO}_2)_2(\text{H}_2\text{O})_2](\text{H}_2\text{O})_2$. *Am. Mineral.* **2011**, *96*, 202–206.
- (75) Kubatko, K.-A.; Unruh, D.; Burns, P. C. Affects of Hydrogen Peroxide on the Stability of Becquerelite. *MRS Online Proc. Libr.* **2005**, *893*, 423–428.
- (76) Shoesmith, D. W. *Used Fuel and Uranium Dioxide Dissolution Studies - A Review*; NWMO Technical Report 2007–03. University of Western Ontario, Canada, 2014.
- (77) Cox, J. D.; Wagman, D. D.; Medvedev, V. A. *CODATA Key Values for Thermodynamics*; Hemisphere Publishing Corp.: New York, 1989.